Korean Journal of Remote Sensing, Vol.21, No.1, 2005, pp.73~81

Topography, Vertical and Horizontal Deformation In the Sulzberger Ice Shelf, West Antarctica Using InSAR

Oh-Ig Kwoun*, Sangho Baek,***, Hyongki Lee**,**
Hong-Gyoo Sohn**, Uk Han*****, and C. K. Shum****

U.S. Geological Survey (USGS), EROS Data Center, SAIC, U.S.A*
Laboratory for Space Geodesy and Remote Sensing, The Ohio State University, U.S.A**
The Department of Civil Engineering, Korea Military Academy, Republic of Korea***
School of Civil & Environmental Engineering, Yonsei University, Republic of Korea****
The Department of Environmental Science, Korea Military Academy, Korea*****

Abstract : We construct improved geocentric digital elevation model (DEM), estimate tidal dynamics and ice stream velocity over Sulzberger Ice Shelf, West Antarctica employing differential interferograms from 12 ERS tandem mission Synthetic Aperture Radar (SAR) images acquired in austral fall of 1996. Ice, Cloud, and land Elevation Satellite (ICESat) laser altimetry profiles acquired in the same season as the SAR scenes in 2004 are used as ground control points (GCPs) for Interferometric SAR (InSAR) DEM generation. 20 additional ICESat profiles acquired in 2003-2004 are then used to assess the accuracy of the DEM. The vertical accuracy of the DEM is estimated by comparing elevations with laser altimetry data from ICESat. The mean height difference between all ICESat data and DEM is -0.57 m with a standard deviation of 5.88 m. We demonstrate that ICESat elevations can be successfully used as GCPs to improve the accuracy of an InSAR derived DEM. In addition, the magnitude and the direction of tidal changes estimated from interferogram are compared with those predicted tidal differences from four ocean tide models. Tidal deformation measured in InSAR is -16.7 cm and it agrees well within 3 cm with predicted ones from tide models. Lastly, ice surface velocity is estimated by combining speckle matching technique and InSAR line-of-sight measurement. This study shows that the maximum speed and mean speed are 509 m/yr and 131 m/yr, respectively. Our results can be useful for the mass balance study in this area and sea level change.

Key Words : InSAR, ICESat Altimetry, GCP, DEM, Ice Velocity, Tidal Deformation.

1. Introduction

Arctic and Antarctic ice sheets preserve more than 77% of the global fresh water and could raise global sea level by several meters if completely melted. Therefore, ice mass balance study in this area has its significance in predicting the sea level and global climate changes. The West Antarctic Ice Sheet exhibits a bimodal behavior, thickening in the west, thinning in the north, but losing mass overall at ~65 km^3/yr, raising sea level by ~0.16

Received 15 December 2004; Accepted 20 January 2005.

mm/yr (Zwally and Giovinetto, 2001). Ocean tides near and under ice shelves shift the grounding line position significantly and are one of current limitations to study glacier dynamics and mass balance. Although grounding line mapping is tedious, it provides the siege of important ice-ocean interactions which are likely to be strongly modulated by tide (Rignot, *personal communication*, 2002). The Sulzberger ice shelf is an area of ice mass flux change in West Antarctica and has not yet been well studied. The Sulzberger Bay is located in front of the Sulzberger Ice Shelf right next to Ross Sea (Fig. 1). It is one of the major drainage outlets of the West Antarctic Ice Sheet, and is characterized by a large glacially carved trough under the ice shelf with depth exceeding 2 km below sea level. The best digital elevation model (DEM) available for Antarctica and for the study area include the Radarsat Mapping Project (RAMP) DEM (Liu *et al.*, 2001). The RAMP DEM has a resolution of 200 m at best; however, for our study area in regions near the edge of land or ice shelf the DEM has significant gaps. ERS-1 radar altimeter DEM has 1 km footprints along its ground track, and the cross-track resolution (from the ERS-1 geodetic mission) is at best 20 km, which are much coarser in resolution than SAR products (pixel resolution of tens of meters). In this study, we use repeat pass SAR interferometric method to generate a DEM and compared it with the the ICESat laser altimeter observed elevation profiles. Improved high resolution DEM can be used for glaciological studies such as ice shelf grounding line estimation for mass balance study. Tidal deformation signal detection and ice surface velocity estimation are important parameters to be considered in grounding line detection and further ice mass balance study. In this study, we use short baseline interferograms for tidal deformation estimation. In addition, ice surface velocity is estimated by speckle matching technique and InSAR line-of-sight measurement to the along track and across track direction, respectively.

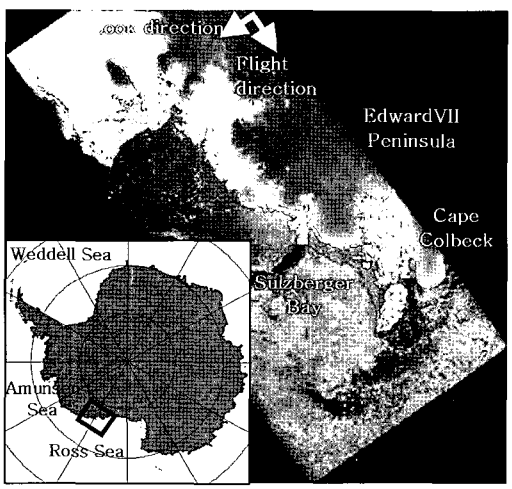

Fig. 1. Geocoded SAR amplitude image (100 km by 200 km) of the study area. The Sulzberger ice shelf area extends -76.5 to -77.5 in latitude and -153 to -156 in longitude.

2. Datasets and Methods

1) SAR Data

ERS1/2 SAR tandem pairs acquired in 1996 are used for DEM generation and grounding line detection. Table 1 shows ERS1/2 tandem data pairs and the associated baseline information.

2) ICESat Data

On 12 January 2003, NASA launched the first Earth

Table 1. ERS1/2 SAR data used in this study(All ascending pass data).

Track	Orbit (ERS1/2)	Acquisition Date	Perpendicular Baseline, m
381	23916/4243	10/11-2-1996	-152.1
	24417/4744	16/17-3-1996	-147.4
	24918/5245	20/21-4-1996	-5.8
424	23959/4286	13/14-2-1996	-120.8
	24460/4787	19/20-3-1996	-194.9
	24961/5288	23/24-4-1996	-22.9

observing satellite laser altimetry mission, ICESat. ICESat's laser footprint diameter is about 70 m and the along-track spacing of 170 m provide much denser elevation data than traditional radar altimetry and ICESat works well over all surface types with moderate slopes. The vertical accuracy of ICESat is projected to be <5 cm rms and the horizontal footprint accuracy is within ±10 m (Zwally and Shuman, 2002). Initial studies have shown that ICESat elevation data are accurate to within ±10 cm (Braun *et al.*, 2004; Magruder *et al.*, 2003).

In this study, we use the Geoscience Laser Altimeter System (GLAS) products GLA06 (global elevations) and GLA12 (Ice sheet elevations) available through National Snow and Ice Datacenter website(http://nsidc.org/daac/icesat/). These data products include a total of 24 profiles from the ICESat laser phases 2a (25 Sep 2003-19 Nov 2003), 2b (17 Feb 2004-21 Mar 2004), and 2c (17 May 2004-19 Jun 2004). Since the radar and laser data were acquired 8 years apart (1996 and 2003-2004), we use 4 ICESat profiles from phase 2b which are acquired in approximately the same season as the ERS SAR scenes, and use the profiles as GCPs in the InSAR processing. The remaining 20 ICESat profiles are then used for DEM validation and, after accounting for elevation changes using geophysical models, they are used to combine with InSAR data to generate a composite DEM.

3) Differential Interferogram

Interferograms between each ERS1/2 tandem pairs (denoted as Interf1 and Interf2 in Fig. 2.) contain both topographic phase and deformation phase corresponding to the observed surface on the ground. A differential interferogram without baseline scaling, denoted as D12 (a) in Fig. 2, contains topographic phase with respect to the baseline difference between the two interferograms. On the other hand, by applying baseline scaling which means integer linear combination between two

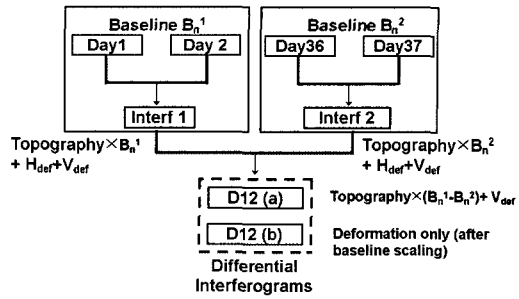

Fig. 2. Diagram for differential interferogram generation (Modified from Fatland and Lingle, 1998).

interferograms, we can have another differential interferogram. The purpose of the baseline scaling is to make the combined baseline close to zero. In this way we can cancel out most of the topographic phase and have deformation-only phase in the resulting interferogram.

Assuming ice motion is linear and constant on the land, two interferograms with the same time span will have the same range difference due to surface displacement. Thus by subtracting two interferograms, topographic phase will remain in differential interferogram. On the ocean, however, range differences are caused by not only horizontal displacements but also vertical displacements. Unlike the horizontal displacement on the land, the vertical displacement (mainly due to ocean tide) is non-linear and even in the differential interferogram vertical displacement cannot be canceled. For that reason we masked out the ocean area including grounding zone and generated a DEM on the land only.

Given two interferograms with almost the same baseline, vertical deformation phase will be dominant in the differential interferogram and it is called "tide interferogram" (Rignot, 1998). The study area can be classified by five areas based on interferograms and SAR amplitude images: land glacier, ice tongue which is floating on sea, grounding zone which is transition area between ground and floating ice, ice stream on land, and sea ice.

3. DEM Generation

The DEM generation technique using the differential interferogram is described by Kwok and Fahnestock (1996). We present a brief scheme for the method applied here as follows:

1) Image Coregistration

To make an interferogram from a pair of single look complex (SLC) images, the two images should be coregistered. The cross-correlation coregistration method is applied. Co-registration offsets are estimated by locating the peak of the cross-correlation between small subsets of image pairs. This procedure is repeated throughout the image to determine the offsets as functions of azimuth and range coordinates. One image is then resampled to be co-registered with respect to the other image based on the offset functions.

2) Interferogram Generation

The interferometric phase values are calculated by subtracting the phase of one image from the other. This is done by multiplying one SLC with a complex conjugate of the other. The interferometric phase at this stage is composed of phase contributions from surface topography, surface deformation, distance between satellites, atmospheric (troposphere and ionosphere) delay, and noise. In addition, the phase computed from the interferogram is in modulo of 2π.

3) Removal of Phase Ramps and Noise

Phase ramps are computed from range differences between satellites and the reference surface such as the Earth ellipsoid model defined by WGS84. The phase ramp is subtracted from the original interferometric phase. To reduce the phase noise in the interferogram, multilooking in 3 by 15 (3 in range direction and 15 in azimuth direction) and phase noise filtering are performed.

4) Phase-unwrapping

To estimate surface elevation from the interferometric phase, modulo 2π ambiguity of the phase needs to be resolved by unwrapping the phase. We applied the branch cut method for this step (*Goldstein et al.*, 1988).

5) Baseline Estimation

Based on the precise orbital parameters, the baseline can be computed. However the calculated baseline is not accurate enough to be used to convert the unwrapped interferometric phase to the height value. To refine the baseline, ground points with known elevations (or ground control points) in the image are used (Zebker *et al.*, 1994). We exploit four ICESat GLAS profiles from the same season as SAR scenes as ground control points.

6) DEM Estimation

Assuming that the surface deformation and atmospheric delays are negligible, the range and the look angle for each pixel in the interferogram are calculated by using the unwrapped phase and refined baseline (*Rufino et al.*, 1998). The range difference with respect to the refined baseline allows us to determine the height difference between arbitrary target points. The DEM derived from the SAR interferometry technique is geocoded into a map coordinate.

Considering a larger baseline ratio between differential interferograms is better for detecting topography, we selected four differential interferograms to construct interferometric DEMs listed in Table 2. Fig. 3 shows their interferograms and the resulting geocoded interferometric DEM over land area.

As can be shown in Table 1, the baseline magnitude from February and March for track 381 is almost the same between two interferograms. This interferogram is used for deformation detection due to their small baseline ratio. From this interferogram with short

Table 2. Differential interferogram pairs.

Image ID	Master pair (ERS1/2)	Slave pair (ERS1/2)	B_p* m	B_T** Days
1	23916/4243	24918/5245	-146.2	35
2	24417/4744	24918/5245	-141.6	70
3	23959/4286	24961/5288	-143.8	35
4	24460/4787	24961/5288	-217.8	70

*B_p : Perpendicular baseline **B_T : Temporal baseline

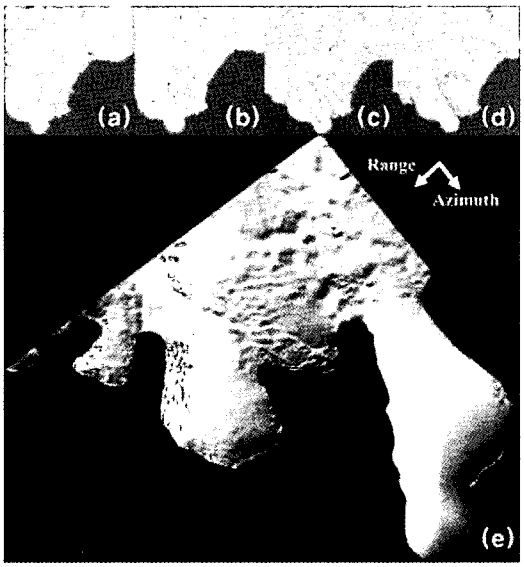

Fig. 3. (a)-(d) Differential interferograms according to the combinations in Table 2. (e) Composite DEM in shade images.

baseline, it is clear to see the grounding line along the coast (Fig. 4(a)). Using both differential interferogram and amplitude images from this track, we classified this area into five areas shown in Fig. 4(b).

4. DEM Validation

To check the quality of the InSAR DEM, we compared the DEM (1996) with ICESat laser altimeter observed elevation profiles (2004). The differences between ICESat and the InSAR DEM are 0.11 ± 6.14 m (mean and standard deviations) for ICESat phase 2a and

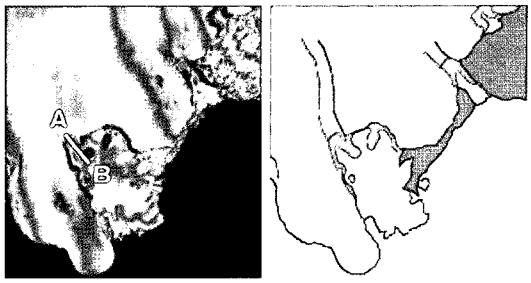

(a) (b)

Fig. 4. (a) Differential interferogram between February and March from track 381. (b) Classification for land glacier (peach), ice tongue (yellow), grounding zone (green), ice stream (cyan), and sea ice (pink).

-1.13 ± 5.48 m for phases 2b & 2c. The difference between all the ICESat profiles and the InSAR DEM is -0.57 ± 5.88 m.

The differences can be attributed to a number of factors. In addition to the above-mentioned assumption that the atmospheric delay anomalies are negligible during the baseline refinement and differential InSAR processing, additional physical processes and error sources exist when combining 1996 SAR data and 2004 ICESat laser altimetry data to derive a DEM. These processes include surface changes or ice dynamics such as ice melt, snow accumulation, and ice flow. Wingham *et al.* (1998) reported that the average elevation change in the Sulzberger Ice Shelf drainage basin has a rate of -3.3 ± 2.6 cm/yr between 1992 and 1996. If this rate persists to the present day, the cumulative elevation change over eight years (1996 to 2004) would be from -6 to -50 cm. Laser altimetry measures the top of snow/ice surface while C-band radar (SAR) could penetrate into the snow/ice cover. The depth of radar penetration can be several meters depending on the wetness and compactness of the ice/snow cover (Hoen and Zebker, 2000 and Rignot *et al.*, 2001). Solid Earth tide deformations have been corrected for laser altimetry, but not for SAR processing. Earth tides produce radial deformations of -14 mm, -58 mm, and +55 mm over the Sulzberger Ice Shelf in February,

March and April 1996, respectively. Glacial isostatic adjustment uplift predicted using an Antarctic model (D91-1.5 model) (Ivins *et al.*, 2001) has a value of about 2 mm/yr, resulting in a maximum of 1.6 cm uplift in 8 years. The atmospheric loading effects are not modeled for neither ICESat nor InSAR, however, is considered small (cms) and negligible. Finally, changes in atmospheric conditions may introduce artifacts in the DEM interferograms. In summary, the combined effects with the exception of unmodeled surface elevation changes is conservatively estimated to be at the meter level and is thus considered to be well within the vertical uncertainty of InSAR DEMs. From the baselines in Table 2., 5.88 m standard deviation (assuming that ICESat profiles represent the ground truth) is equivalent to less than 0.6 radian (about 35 degrees) of phase noise. Therefore, we suggest that the InSAR DEM is reasonably accurate to represent the elevation of the study area in 2004.

5. Tidal Deformation Detection

As shown in the Fig. 4 and in the floating ice shelf area, due to the tidal differences between successive images, there are dense fringe lines (so called 'fringe belts') along the transition area from land to sea in the differential interferogram. We examine the consistency of the tidal change between available ocean tide models and SAR interferogram over the time span for SAR data acquisition.

As shown in Table 3, four tide models are used for comparison (Matsumoto *et al.*, 2000; Egbert *et al.*, 2002; Padman *et al.*, 2002; Ray, 1999). Among these models, there are no significant differences in magnitude and direction of tides corresponding to each SAR data acquisition time. This is as expected for global models NAO, TPXO and GOT99 as they are primarily constrained by the FES94 hydrodynamic model for the regions outside of $\pm 66^0$ latitude. Each predicted tidal

Table 3. Tidal difference by model at 77.167S and 156.667W.

Date	Geocentric tide (cm)				Solid Earth
	NAO	TPXO	CATS	GOT	Tide (cm)
1996-2-10	-15.8	-13.1	-12.3	-7.4	-0.7
1996-2-11	-21.5	-21.1	-20.1	-15.6	-0.3
1996-2-13	-24.1	-24.3	-23.8	-23.8	-0.9
1996-2-14	-20.1	-16.7	-16.7	-20.4	-2.2
1996-3-13	-36.6	-33.0	-31.9	-31.3	-0.7
1996-3-14	-28.7	-22.2	-21.9	-24.8	-2.6
1996-3-16	-9.8	2.9	1.6	-8.6	-5.8
1996-3-17	-0.8	12.5	10.8	-3.1	-6.2
1996-4-17	-10.7	-5.2	-7.0	-16.2	-0.2
1996-4-18	-17.6	-15.5	-16.3	-22.2	2.0
1996-4-23	-49.7	-52.6	-51.3	-36.0	5.3
1996-4-24	-47.2	-48.5	-47.9	-33.4	4.2

difference by these models is presented in Table 4. These values represent relative tidal change between day 1 and day 37 (see Fig. 2).

Negative value means the sea level on day 37 is lower than that on day 1. Tidal differences measured by SAR interferometry are obtained by the phase difference between A and B marked on Fig. 4(a). Phase values in the unwrapped interferogram are 0.12 rad and 34.66 rad for A and B correspondingly. This range difference (Δr) is converted to a sea surface elevation change (Δz) using (Rignot *et al.*, 2000)

$$\Delta z = \frac{\Delta r}{\cos \alpha}$$

where α indicates the incidence angle for object. For ERS satellite, this angle is about 23° for this area. According to above equation, range difference 34.54 rad

Table 4. Relative tidal changes including solid earth tide by tide model.

Model	Relative tidal changes including Solid Earth Tide (cm)
NAO	-13.9
TPXO	-16.7
CATS	-16.1
GOT	-13.1

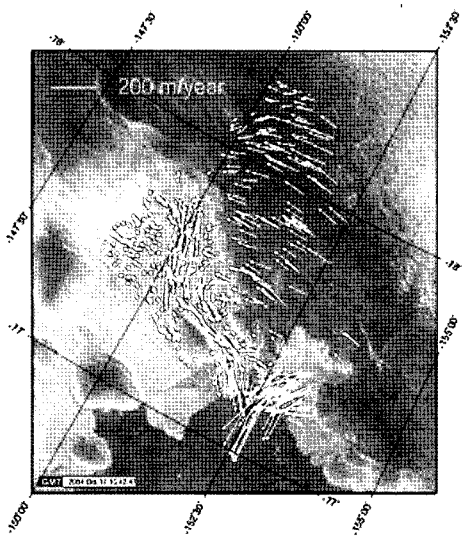

Fig. 5. Estimated ice surface velocity.

is converted into vertical displacement 37.52 rad. This value is difference for round trip so after dividing by two and multiplying 5.6 cm / 2π (wave length of ERS is 5.6 cm), we get 16.7 cm as a sea surface elevation change. A positive value means subsidence of the surface in image from day 37 relative to in image from day 1. So the magnitude and its direction agree with those predicted from tide models. Among four tide models, TPXO and CATS models fit well. However, the inverse barometric (IB) effect is not adjusted for this data, yet.

6. Ice Surface Velocity Estimation

The typical InSAR technique can measure the velocity of glacier only in the line-of-sight direction if only one InSAR pair is available. In this study, speckle matching technique is applied to measure the azimuth direction velocity. The speckle matching technique is based on cross-correlation matching operation to calculate the range and azimuth offsets which contain the surface displacement information. Since the range velocity calculated by InSAR method gives us better accuracy than by Speckle Matching method, we can combine both methods to generate two-dimensional surface velocity. Range velocity is detected by a tandem pair of ERS-1 23959 and ERS-2 4286. On the other hand, azimuth velocity is estimated by speckle matching technique. We could hardly find any known velocity control point over the study area, the flow direction observed by the flow stripes in the imagery is used as control data. Fig. 5 shows ice surface velocity for the study area. This study demonstrates that the maximum speed in this area is ~509 m/year and mean speed is ~131 m/year.

7. Conclusions

In this study, we generated a digital elevation model near the Sulzberger ice shelf using SAR interferometry and ICESat GLAS profiles. The difference between ICESat profiles and the InSAR DEM was -0.57 $\pm$ 5.88 m. However, the fact that the DEM excludes the floating ice may limit the broad usage of the land-only DEM for glaciological studies and DEM over floating ice tongue is left for further study. The comparison of tidal differences between tide models and InSAR measurement shows a good agreement. The grounding zone along the ice tongues in this area was mapped using interferograms. Ice surface velocity was estimated by combining range and azimuth direction velocity. We conclude that InSAR technique is useful in DEM generation, tidal change detection, and ice surface velocity estimation in this area. In addition, we find that ICESat elevation data are very important for accurate InSAR DEM estimation on regions where no ground control points are available, such as polar regions. Our efforts in this study have contribution to the mass balance study in this area and further to the climate changes caused by sea level rise.

Acknowledgments

The copyright for ERS1/2 data belongs to the European Space Agency (ESA) and data is provided by Alaska Satellite Facility (ASF). We thank Laramie Potts from Laboratory for Space Geodesy and Remote Sensing, The Ohio State University for his careful review. This research is supported by a grant from the National Science Foundation Office of Polar Program (OPP -0088029).

References

Braun, A., K. Cheng, B. Csatho, and C. Shum, 2004. ICESat laser altimetry in the Great Lakes, *Proc. Institute of Navigation (ION) 60th Ann. Meeting*, Dayton, Ohio, USA.

Egbert, G. D. and L. Erofeeva, 2002. Efficient inverse modeling of barotropic ocean tides, *J. Atmos. Oceanic Tech.*, 19.

Fatland, D. R. and C. S. Lingle, 1998. Analysis of the 1993-95 Bering Glacier (Alaska) surge using differential SAR interferometry, *J. Glaciol*, 44(148): 532-546.

Goldstein, R. M., H. A. Zebker, and C. L. Werner, July-August 1988. Satellite radar interferometry: two-dimensional phase unwrapping, *Radio Science*, 23(4): 713-720.

Hoen, E. and H. Zebker, 2000. Penetration depths inferred from interferometric volume decorrelation observed over the Greenland ice sheet, *IEEE Trans, Geosci, Remote Sens.*, 38: 2571-2583.

Ivins, E., X. Wu, C. Raymond, C. Yoder, and T. James, 2001. Temporal Geoid of a Rebounding Antarctica and Potential Measurement by the GRACE and GOCE Satellites, *IAG Symposia, vol. 123, GGG2000* (M. Sideris, ed.), Springer-Verlag, Berlin Heidelberg, pp. 361-366.

Kwok, R. and M. A. Fahnestock, 1996. Ice Sheet Motion and Topography from Radar Interferometry, *IEEE Trans, Geosci, Remote Sens.*, 34(1): 189-200.

Liu, H., K. Jezek, B. Li, and Z. Zhao, 2001. Radarsat Antarctic Mapping Project digital elevation model version 2. Boulder, CO: National Snow and Ice Data Center. Digital media.

Magruder, L. A., B. E. Schutz, and E. C. Silverberg, 2003. Laser pointing angle and time of measurement verification of the ICESat laser altimeter using a ground-based electro-optical detection system, *J. Geodesy*, 77(3-4): 148-154.

Matsumoto, K., T. Takanezawa, and M. Ooe, 2000. Ocean Tide Models Developed by Assimilating TOPEX/POSEIDON Altimeter Data into Hydrodynamical Model: A Global Model and a Regional Model Around Japan, *J. Oceanog.*, 56: 567-581.

Padman, L., H. A. Fricker, R. Coleman, S. Howard, and S. Erofeeva, 2000. A new tidal model for the Antarctic ice shelves and seas, *Ann. Glaciol.*, 34: 247-254.

Ray, R. D., 1999. A Global Ocean Tide Model From TOPEX/POSEIDON Altimetry: GOT99.2, *NASA Technical Memorandum 209478.*

Rignot, E., 1998. Hinge-line migration of Peterman Gletscher, north Greenland, detected using satellite-radar interferometry, *J. Glaciol.*, 44(148): 469-476.

Rignot, E., L. Padman, D. R. MacAyeal, and M. Schmeltz, 2000. Observation of ocean tides below the Filchner and Ronne Ice Shelves, Antarctica, using synthetic aperture radar interferometry: Comparison with tide model predictions, *J. Geophys. Res.*, 105: 19,615-19,630.

Rignot, E., K. Echelmeyer, and W. Krabill, 2001. Penetration depth of interferometric synthetic-aperture radar signals in snow and ice, *Geophys. Res. Lett.*, 28(18): 3501-3504.

Rufino, G., A. Moccia and S. Esposito, 1998. DEM generation by means of ERS tandem data, *IEEE Trans. Geosci. Remote Sens.*, 36(6): 1,905-1,912.

Wingham, D., A. Ridout, R. Scharroo, A. Arthern, and C. Shum, 1998. Antarctic Elevation Change from 1992 to 1996, *Science*, 282: 456-458.

Zebker, H. A., C. L. Werner, P. A. Rose, and S. Hensley, 1994. Accuracy of topographic maps derived from ERS-1 interferometric Radar, *IEEE Trans. Geosci. Remote Sens.*, 32(4): 823-836.

Zwally, H. J. and M. B. Giovinetto, 2001. Balance Mass Flux and Ice Velocity Across the Equilibrium Line in Drainage Systems of Greenland, *J. Geophys. Res. (Atmospheres)*, 106(D24): 33,717-33,728.

Zwally, H. J. and C. Shuman, 2002. *ICESat: Ice, Cloud, and land Elevation Satellite, Brochure FS-2002-9-047-GSFC*, 23 pp, NASA/ GSFC, Greenbelt, Maryland, USA.